Fast, immiscible fluid-fluid displacement in three-dimensional porous media at finite viscosity contrast

Vidar Frette, Jens Feder, Torstein Jøssang, Paul Meakin,
and Knut Jørgen Måløy
Department of Physics, University of Oslo, P.O.Box 1048 Blindern, N-0316 Oslo, Norway
(Received 21 March 1994)

The crossover from capillary to viscous flow during immiscible fluid-fluid displacement has been studied in transparent, three-dimensional porous media. The defending and the invading fluids have equal densities, so that gravity effects are eliminated. The viscosity ratio of defending fluid to injected fluid m is moderate $m \simeq 14$. Dense, ball-like displacement structures are generated at high injection rates. Surprisingly, the flow appears to be nearly completely stabilized even though the viscosity of the invading fluid is significantly lower than that of the defending fluid. For the physical system studied here, fully developed ball-like patterns arise for capillary numbers $\mathrm{Ca} \geq 5 \times 10^{-3}$. A similar behavior is found in experiments using the same grains and fluids in a two-dimensional system.

PACS number(s): 47.55.Mh, 47.55.Kf, 05.40.+j, 47.20.Hw

I. INTRODUCTION

Immiscible fluid-fluid displacement processes in porous media provide a rich "laboratory" for experimental investigation of a variety of general issues in statistical physics. The displacement fronts are sensitive to the quenched (local) randomness of the porous medium (variations in pore sizes, pore neck sizes, wettability, pore wall roughness, and large scale heterogeneities), as well as imposed (global) fields such as pressure and gravitational fields. These fields may couple to the instantaneous position of the displacement front. As a result of the competition between the effects of the local disorder and fields, a variety of front morphologies may be generated. Many of them are related to growth processes in quite different physical systems. In some cases the displacement fronts have a fractal geometry.

Many commercially important processes involve the simultaneous flow of several immiscible fluids through a porous medium. Important examples include motion of the ground water table in soils or sands, the flow of hydrocarbons and water through porous rocks during oil recovery, the drying of amorphous materials, and water purification by filtration through sand beds. Many approximate schemes [1–3], involving phenomenological concepts such as relative permeabilities, have been developed to understand fluid-fluid displacement processes like these. However, the results obtained from these models are often inconsistent with experimental observation of fractal displacement fronts [4] and our understanding of front propagation processes is far from complete.

Here attention is focused on a drainage process (in which a nonwetting fluid invades a porous medium saturated with an immiscible wetting fluid) at a moderate viscosity contrast and high displacement rates. Previous work on drainage, both in certain limiting cases (regimes) and more specifically at low viscosity contrast (important for many applications), is discussed below. An advantage of the experiments to be reported here is that fast fluid-fluid displacement has been visualized in large *three-dimensional* porous media, whereas most previous experimental work has been on quasi-two-dimensional systems. Further, gravity effects are eliminated from the system since fluids with equal densities are used. Surprisingly stable and dense structures are formed at high displacement rates (see Figs. 2 and 3). The patterns are strikingly different from the ramified structures which are usually generated in unstable displacements.

At a finite viscosity contrast crossover morphologies, with structures that are intermediate between those generated in the more easily understood limiting cases, are expected. For a review of different flow regimes see Ref. [5]. Two kinds of forces are relevant for the two-fluid displacement process considered here: viscous forces and capillary forces.

The *slow* ($\mathrm{Ca} \ll 10^{-4}$) penetration of a nonwetting fluid into porous medium saturated with a wetting fluid of the same density is dominated by capillary forces. (The ratio of viscous to capillary forces is characterized by the capillary number $\mathrm{Ca} = \frac{\mu v}{\sigma}$, where μ is the viscosity of the defending fluid, v a characteristic front velocity, and σ the interfacial tension.) Such a flow will be sensitive only to the quenched randomness associated with the medium. This process generates patterns with a geometry and dynamics that can be described by the invasion percolation model [6–14].

Viscous effects dominate in gravity-free two-fluid displacement at high displacement rates ($\mathrm{Ca} \gg 10^{-4}$). If the viscosity of the defending fluid is much higher than the viscosity of the invading fluid ($m \gg 1$), such as when a high viscosity liquid is being displaced by a gas, only viscous pressure drops in the defending fluid are of importance. This unstable situation leads to ramified patterns that can be described by the diffusion-limited-aggregation (DLA) model [15–21]. Both in the fast ex-

periments and the DLA model the growth of the pattern is concentrated on its outmost tips [22, 23].

The systematic changes in pattern morphology with increasing capillary number has been investigated theoretically in the limit in which the invading fluid has zero viscosity ($m \gg 1$) [24]. Experiments indicate that the viscosity ratio m has little influence on invasion percolation, but may be important at high displacement rates. For low m the viscous pressure drops in the two fluid phases are comparable and must both be taken into account to understand the dynamical behavior of the interface. Several numerical and a few experimental studies of the effects of the viscosity ratio on the morphologies of displacement patterns have been reported.

Numerical approaches include solving for the pressure field in both fluid phases with a homogeneous medium [25–29] and computation of displacement processes in large networks of tubes [30–33]. Encouraged by the success of the DLA model in dealing with the high viscosity contrast limit, several workers have consider extensions of this model incorporating a finite viscosity contrast [34–40]. The hope has been that a modified DLA algorithm could be much faster computationally than a full solution of the flow problem. Computation time is crucial for large simulations on realistic geometries, e.g., permeability variations and layers (see Ref. [35]), or spot configurations. Unfortunately, modifications of the DLA model to simulate more general fluid-fluid displacement processes tend to increase the computation time significantly.

The approximations used in the computer models have not all been sufficiently justified and detailed experimental verification is, to a large extent, lacking. Another limitation of most of the models is that they do not contain any parameter corresponding to the displacement velocity. Thus they are unable to account for the increasing influence of capillary effects at lower displacement rates. Several of the models mentioned above do not contain interfacial tension. However, some overall features have emerged from these studies. As the viscosity ratio fall from a very large value towards 1 fewer, shorter, and thicker fingers are generated. In the limit $m \to 1+$ the pattern formed by the invading fluid is compact. Simulations [30, 31, 38, 39] detail the falloff of the effective surface dimension of patterns as a function of the viscosity ratio. An important *dynamical* consequence of a finite viscosity ratio is that the invading fluid structure continues to evolve after breakthrough to ambient pressure [29].

Dense patterns for the viscous regime were found in drainage experiments at $m \simeq 45$ in a consolidated quasi-two-dimensional packing of glass beads [41]. In a series of experiments in two-dimensional etched networks using many viscosity ratios and displacement rates a tendency to form denser patterns as $m \to 1+$ was observed, but the low-m regime was not treated in detail [42–44]. More dense structures were also generated as m decreased in a series of experiments in a monolayer of glass beads [45]. Finger patterns generated in three-dimensional porous media at low viscosity contrasts have been visualized using index matching techniques [46, 47].

II. EXPERIMENTAL SYSTEMS

The two- and three-dimensional porous media used were packings of Plexiglas (polymethylmethacrylate) grains (Röhm Formmasse 7N Glasklar). The grains were 2 mm diam, 2 mm long cylinders with volumes $v_g \simeq 6.3\,\mathrm{mm}^3$. Dibutyl-phthalate was chosen as the defending fluid, since it has an index of refraction ($n = 1.491$) that matches that of Plexiglas at room temperature. The porous media constructed in this manner become transparent when saturated with this liquid and a second fluid phase can be observed directly. The invading fluid (the fluid to be injected) was a solution of 11.8 wt. % sucrose in water. This liquid was chosen since it has a density ρ equal to that of dibutyl-phthalate ($\rho = 1.047\,\mathrm{g/cm}^3$) so that the effects of gravity were eliminated. The injected liquid was dyed black with negrosin 1 g/kg in order to get good visual contrast. A solution of sucrose in water is highly polar and therefore immiscible in dibutyl-phthalate. The viscosity of the sucrose solution was $\mu_i = 1.45\,\mathrm{cP}$ and the viscosity of dibutyl-phthalate was $\mu = 20.7\,\mathrm{cP}$. The viscosity ratio m between defending (displaced) and invading (injected) fluid was $m = \mu/\mu_i = 14$. Dibutyl-phthalate is the wetting fluid. However, wetting properties may vary at grain surfaces exposed to the sucrose solution for a long period; they become less preferably wetted by dibutyl-phthalate. The interfacial tension σ between the fluids was estimated to be $13 \pm 1.5\,\mathrm{dyn/cm}$ [48] using a version of the drop weight method [49]. All measurements were made at 20 °C.

The three-dimensional models were unconsolidated packings in a glass container of size $29 \times 29 \times 29\,\mathrm{cm}^3$ or $145 \times 145 \times 145\,\delta^3$ in terms of the grain size $\delta = 2\,\mathrm{mm}$. Unconsolidated packings were used in order to be able to recycle the dibutyl-phthalate. In a consolidated medium it would be difficult to remove the nonwetting phase after each run. The changes in wetting properties with time (see above) is one reason why new grains were used for each experimental run. In order to avoid trapping of air bubbles in the medium the packing process was performed as follows. The necessary amount of liquid was poured into the container. The grains were slowly slid down a smooth, inclined surface into the liquid. The upper parts were slightly stirred during the building up of the medium. The density of polymethylmethacrylate ($\rho = 1.18\,\mathrm{g/cm}^3$) is close to that of dibutyl-phthalate ($\rho = 1.047\,\mathrm{g/cm}^3$). A porosity ϕ of 0.37 was measured for these packings and the medium contained on the order of 2.4×10^6 grains. Using the measured porosity and assuming that there are as many pores as grains in the model, the volume of a typical pore was estimated to be about $v_p \simeq 3.7\,\mathrm{mm}^3$. The models used for experiments were not shaken. The porosities of smaller test packings were reduced by about 5% when shaken. Before filling the container a tube was fixed in position so that the sucrose solution could be injected from a "point" source in the middle of the medium. The packings were loaded with weights on top of a plate during fast displacement experiments to prevent grain movements. The spacing between the top plate and the container wall was about 0.5 cm. A sketch of the setup is shown in Fig. 1.

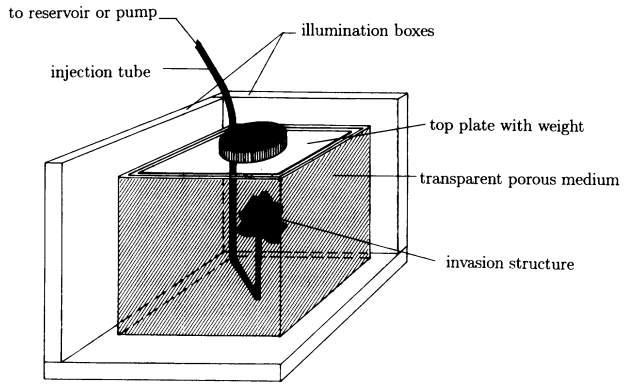

FIG. 1. Experimental setup. A transparent porous medium is held in a glass container. The plate on top of the medium is loaded with a weight to prevent grain movements during the displacement processes. The system is illuminated from below and through two adjacent faces. Two projections of the patterns that are generated when a second fluid is injected are photographed.

Special precautions were taken in the case of slow displacement. The displacement process, in this case, is susceptible to "defects" in the packing and growth will tend to occur along the injection tube. Therefore a thin (about 0.5 mm diameter) and flexible injection tube was used. The open end of the injection tube was supported by thin treads during the packing process described above.

Two-dimensional models were constructed by packing a monolayer of grains in a circular Hele–Shaw cell, i.e., held between two circular plates. An air overpressure was applied to a plastic film below the monolayer to keep all the grains fixed (see Ref. [21]). The diameter of the models was 40 cm. The injected fluid entered the model via the center point. The outer rim of the system was open to the atmosphere. The porosity of these two-dimensional systems were determined to be $\phi = 0.43$ by weighing the amount of grains used. Assuming that there are as many pores as grains in the model the volume of a typical pore was estimated to be $v_p \simeq 4.8\,\mathrm{mm}^3$.

III. EXPERIMENTS

Typical displacement patterns generated in two-dimensional and three-dimensional systems are shown in Figs. 2 and 3, respectively. In these figures each line shows the structures at several stages in one experiment. A constant injection rate was used in each run, and the rates are indicated in the figures. The rates are given in terms of pore volumes per second, and these pore volumes are the characteristic volumes determined in Sec. II above.

The injection in two and three dimensions was performed using a Pharmacia (Uppsala, Sweden) P-500 cromatographic pump for the lowest rates, and a Seybert & Rahier (Immerhausen, Germany) R 410 LWF membrane pump (an industrial dosage pump) was used for intermediate rates. The membrane pump outlet was connected to two (partially air-filled) chambers in series for pulse compensation. By choking the flow after the last chamber a steady output was obtained. For the highest rates hydrostatic pressure was used for injection into the porous medium and the rate was then determined from the weight change of the liquid container (reservoir) and the elapsed time. In these cases the tube was choked by tightening a clamp around it before it entered the experimental system to ensure a constant flow rate through an experiment. For the fastest three-dimensional experiments the reservoir was placed three floors (13 m) above the laboratory. Logging of the container weight during several experiments confirmed that the injection rates were constant to a good approximation. Thus a dominating part of the flow resistance (from the pump or reservoir to the top of the porous medium; see Fig. 1) lies before the porous medium, and changes as the experiment develops and the fluid-fluid interface propagates are insignificant.

The three-dimensional system was illuminated from below and from two "rear" sides and photographed in two projections; see Fig. 1. The cameras were triggered simultaneously and manually to adjust the intervals and compensate for the continuous decrease of the interface velocity in this radial geometry. The horizontal two-dimensional system was illuminated from below and photographed from above. To record the time, clocks were photographed together with the physical models. The total injected fluid volume at the different stages was determined from the elapsed time and the flow rate.

Some of the complex two-dimensional patterns were digitized before further analysis; see below. However, here the main interest was in the limiting case of fast displacement in the three-dimensional system [the lowest two lines in Fig. 3], where there is not much structure left in the pattern. A projection of the main structure onto a plane is, to a good approximation, a growing circle. Therefore the diameters for these patterns were determined by direct measurement on $13 \times 18\,\mathrm{cm}^2$ photographic prints. Typical log-log plots of structure diameter as a function of structure mass are shown in Fig. 4. The clocks used had an resolution only in seconds; therefore it was difficult to determine the start of the injection accurately enough for the highest injection rates [the fastest experiment, the bottom line of Figs. 3 and 4(d), lasted only 12 sec]. For these experiments the times were first determined on a rough second scale. Subsequently the data were adjusted by making use of the fact that the growth should approximately follow a relationship of the form $t \propto M \propto R^D$. Here t is the time since the start of the experiment, M the mass, and R the linear size (radius) of the pattern. A more accurate injection time was determined from

$$\left(\frac{R_1}{R_2}\right)^D = \frac{t_1 - \Delta t}{t_2 - \Delta t}, \tag{1}$$

where R_1 and R_2 are the radii of the first and second patterns, t_1 and t_2 are the times corresponding to the first and second patterns on the approximate scale, and Δt is the shift required to obtain times measured from

the estimated start time. The shifts were found to be in the interval $0.3 < \Delta t < 0.8$ sec. The value $D = 2.76$, obtained from the relatively slow experiments [corresponding to Figs. 4(a) and 4(b)], which had a sufficient time resolution and the times were not adjusted, was used. As is evident in the plots the time resolution problem is most serious for the fastest experiment. Figure 5 shows a similar log-log plot for a very slow experiment. The cluster sizes were determined from photographic prints. In all the three-dimensional experiments measurements of size from two perpendicular projections were averaged for each pattern.

In order to compute the capillary and Reynolds numbers for these processes a characteristic front velocity must be defined. The average velocity of the displacement front from the start of the injection until the diameter of the structure is half the size of the container was chosen. Up to this size the displacement patterns stay approximately spherical. The upper line of Fig. 6 shows (to the right) a displacement structure that fills 80% of the glass container. The overall shape here clearly deviates from being quasispherical. Figure 6 also illustrates some other limitations of the experimental method. For the two-dimensional experiments the capillary numbers (given in Fig. 2) were determined using the average velocity from the start of the experiment until the structure diameter had grown to one-half of the cell diameter.

The radial geometry used in these flow visualizations

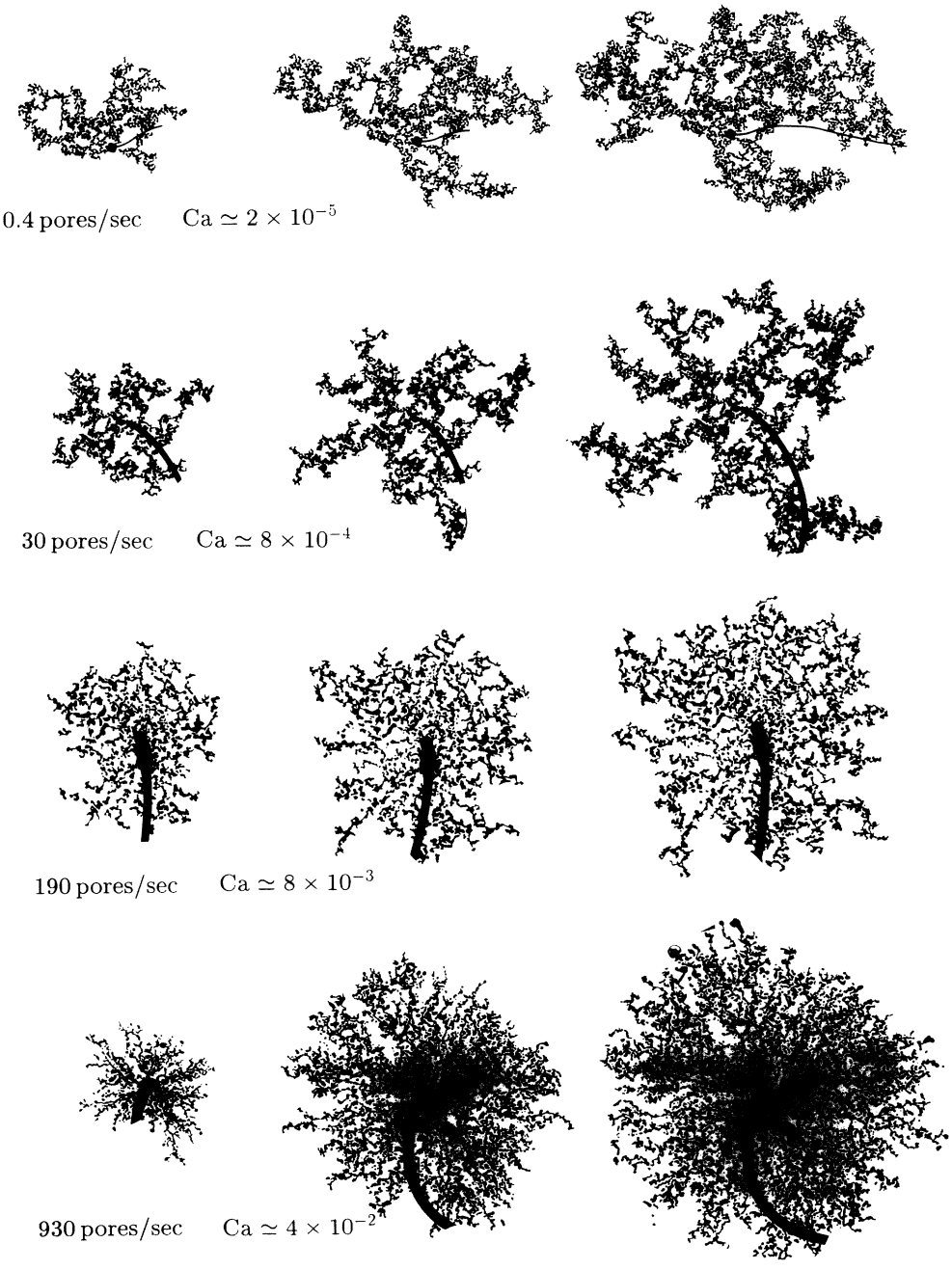

FIG. 2. Fluid-fluid displacement patterns generated in a two-dimensional porous medium. Each line show several stages in one experiment. The injection rates and the values of the capillary number Ca are given in each case. The physical flow rates were 0.007, 0.48, 3.2, and 15.6 l/h.

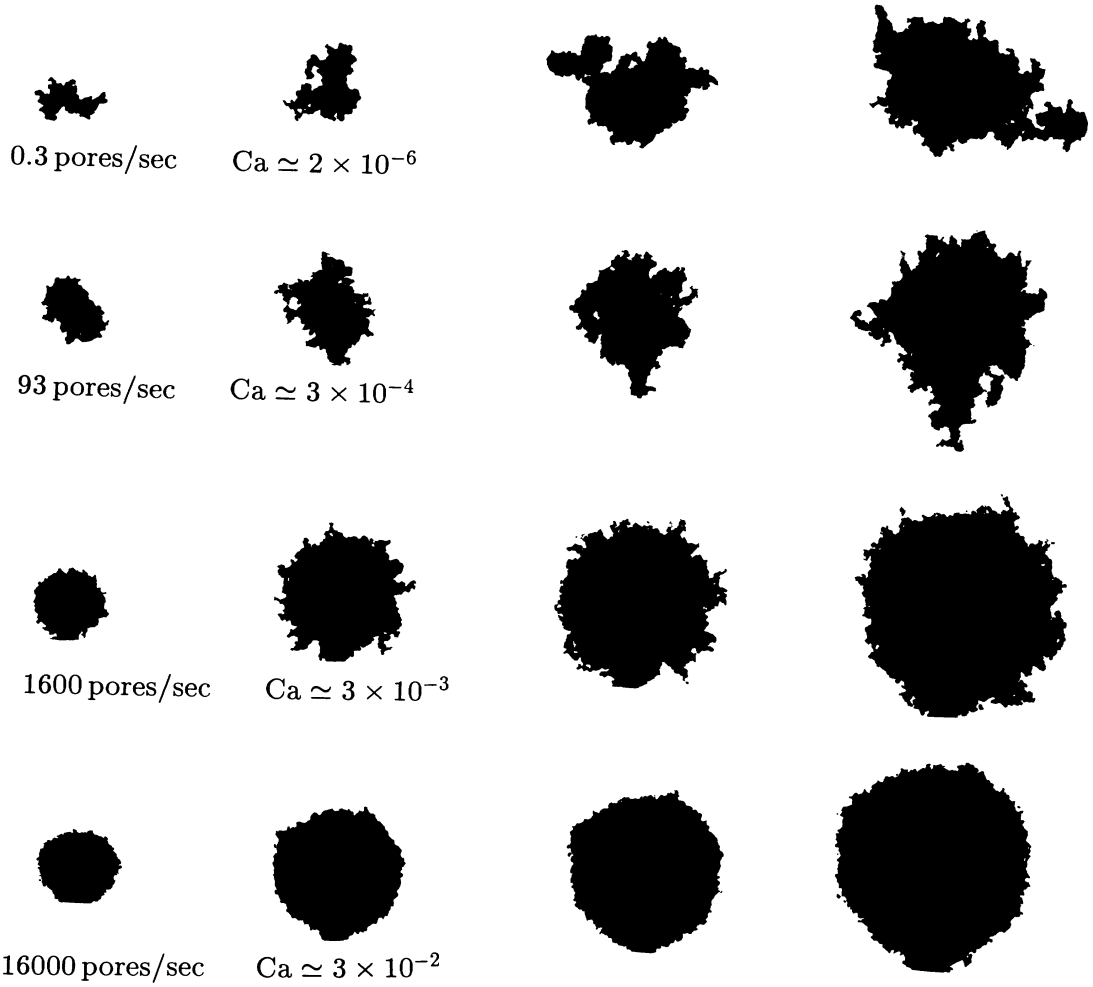

FIG. 3. Fluid-fluid displacement patterns generated in a three-dimensional porous medium. Each line show several stages in one experiment. The injection rates and the values of the capillary number Ca are given in each case. The physical flow rates were 0.004, 1.24, 21, and 210 l/h.

allowed direct observation of the outer surface of the three-dimensional structures. An important limitation, however, is that the capillary number is not constant throughout an experiment but falls off rapidly. The values for the capillary number given in the figures were determined from the *average* front velocity. Since the flow rate was constant, the cluster mass always grew linearly with time t and the instantaneous value for the capillary number Ca behaved like

$$\mathrm{Ca} \propto v = \frac{dR}{dt} \propto \frac{d}{dt} t^{1/D} = t^{1/D-1} = t^{-0.6}, \qquad (2)$$

where R is cluster radius and the exponent value $D = 2.74$ has been inserted. In two dimensions the falloff of Ca with time will occur with a different exponent. Consequently, some caution should be shown when comparing Ca values in two and three dimensions (the Ca values referred to elsewhere in this paper were obtained by averaging as described above).

IV. DISCUSSION

Figure 3 summarizes the main results; it shows the projections of patterns generated during fluid-fluid displacement in three-dimensional porous media at a series of injection rates. For comparison a corresponding series of experiments using the same grains and fluids to construct two-dimensional systems is shown in Fig. 2. These experiments serve as a reference in the present context and have not been analyzed in detail. The qualitative changes in two and in three dimensions are the same as the injection rate is increased. The patterns at low rates grow in sudden bursts (i.e., neighboring pores tend to be invaded in sequence) [12–14] and they show no memory of the injection point [11]. At higher rates structures centered around the injection point are generated and the patterns become increasingly symmetrical and dense as the rate is increased. The surface roughness gives a measure for a characteristic length, which is seen to decrease with increasing rate. For the very slow experiments this length is in principle infinite, whereas it is quite short for the fastest three-dimensional pattern (the bottom line in Fig. 3). The main interest in the present paper is in the crossover to ball-like displacement structures generated at high rate in three dimensions, but the low rate patterns will be discussed first.

The two-dimensional low rate patterns in the upper

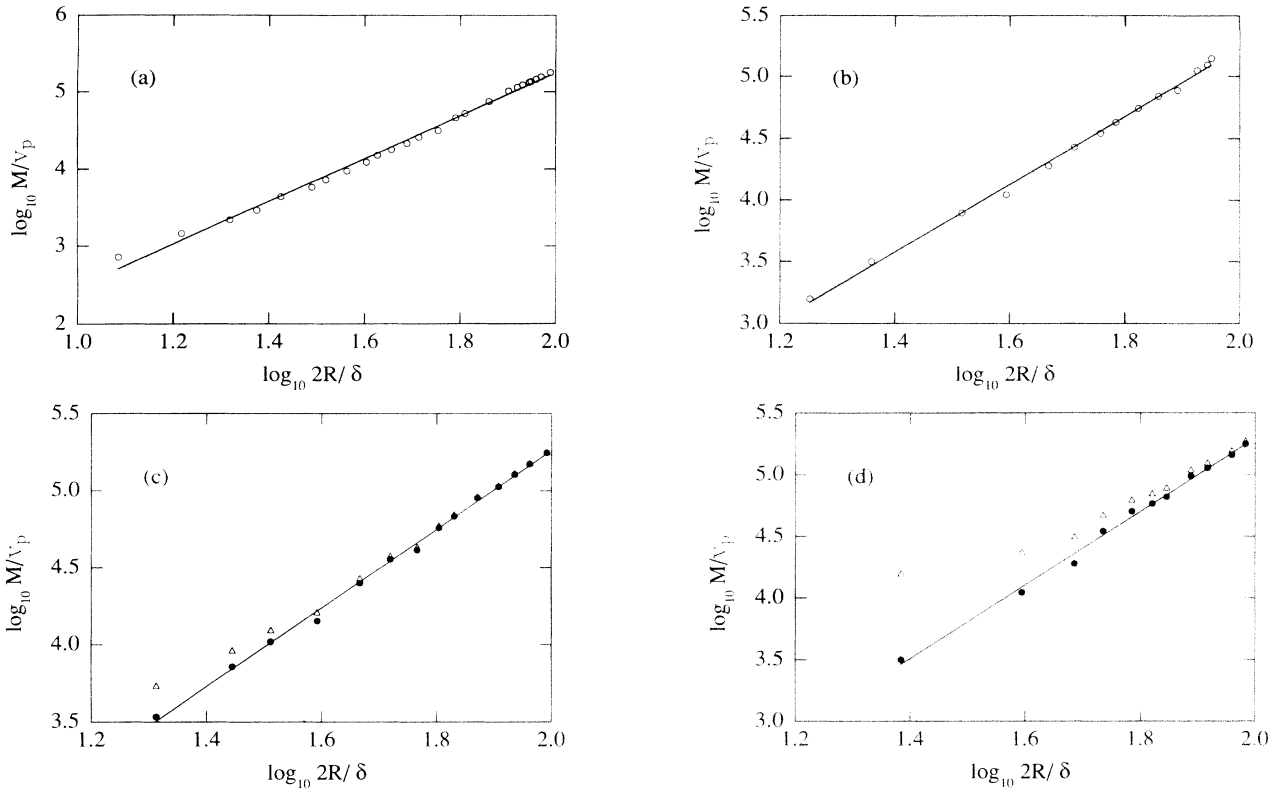

FIG. 4. Log-log plots of the cluster mass M as a function of the linear size $2R$ of their projections (averages from two projections) for fast fluid-fluid displacement in a transparent, three-dimensional porous medium. The diameter $2R$ of these almost spherical structures was used as the measure for linear size. The mass is given in terms of the characteristic pore volume v_p, and the diameters in terms of the grain size δ. The exponent D, where $M/v_p \propto (2R/\delta)^D$, was estimated in each case. In (c) and (d) both adjusted (see Sec. III) data (filled circles) and unadjusted data (open triangles) are plotted. The injection rates, the capillary numbers Ca, the Reynolds number, and the values of the exponent D were:
(a) 720 pores/sec = 9.6 l/h, Ca $\simeq 1 \times 10^{-3}$; Re $\simeq 1.0$, and $D = 2.77 \pm 0.04$.
(b) 1 600 pores/sec = 21 l/h, Ca $\simeq 3 \times 10^{-3}$, Re $\simeq 2.3$, and $D = 2.75 \pm 0.04$ (third line in Fig. 3).
(c) 5400 pores/sec = 72 l/h, Ca $\simeq 9 \times 10^{-3}$, Re $\simeq 8.3$, and $D = 2.56 \pm 0.04$.
(d) 16 000 pores/sec = 210 l/h, Ca $\simeq 3 \times 10^{-2}$, Re $\simeq 24$, and $D = 2.98 \pm 0.07$ (fourth line in Fig. 3).

line of Fig. 2 develop holes of many sizes. The pattern was observed to grow in bursts similar to those associated with the invasion percolation model. A dimension $D = 1.82 \pm 0.1$ was found by analyzing digitized images from two experimental series using the formula $M \sim R_g^D$. Here M is cluster mass and R_g is the cluster radius of gyration. This value for D is consistent with that found in Ref. [11] for invasion percolation experiments.

In contrast to the two-dimensional systems, where there is access to the complete structure geometry, it is necessary to work with the structure *projections* in three-dimensional experiments. The upper line in Fig. 3 shows typical projections of three-dimensional patterns generated during slow flow. Their shapes are irregular, particularly in the early stages. As more and more of the structure is shielded, the projection appears more regular. The early projected patterns contain more holes than the later patterns. The growth appears to come in the form of added "blobs." Traces of burstlike growth can also be seen as steps in Fig. 5, which shows the cluster mass (or time) as a function of cluster size.

Figure 5 gives an estimate $D \simeq 2.7 \pm 0.1$ for the dimensionality of the slow experiment in three dimensions shown in Fig. 3 (upper line). This value is higher than the dimension $D = 2.52$ found for three-dimensional invasion percolation clusters [10]. The value of the exponent obtained from a single experiment is quite sensitive to fluctuations in the growth process. Further, slow flow without gravity is very sensitive to imperfections in the medium, such as the wetting heterogeneity mentioned in Sec. II. Indeed, less preferable wetting by the defending fluid after long exposure to the invading fluid should lead to facilitated invasion in the interior of the structure and more compact growth. In general, a slow fluid-fluid displacement will be dominated by any inhomogeneity in the medium, such as a more loosely packed layer. It is not possible to be certain that a pattern formed by slow flow in three dimensions was not dominated by inhomogeneities. A better approach is therefore to introduce a controlled perturbation as a *parameter*. This perturbation will introduce a length scale and therefore a cutoff into the problem. For a range in this parameter the introduced perturbation may dominate unknown perturbations and account for the cutoff in the process. It may

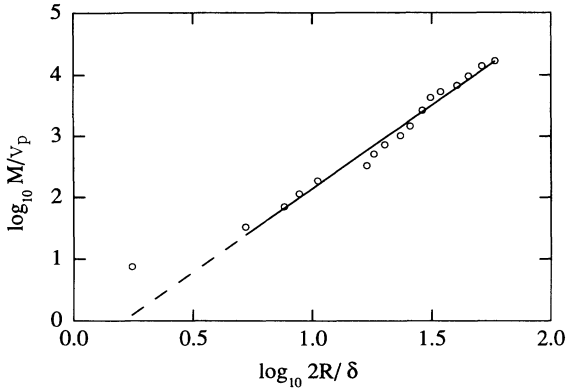

FIG. 5. Log-log plot of the cluster mass M as a function of the linear size $2R$ of their projections (averages from two projections) for very slow fluid-fluid displacement in a transparent, three-dimensional porous medium (first line in Fig. 3). The average of two perpendicular diameters was used as the measure for linear size $2R$. The mass is given in terms of the characteristic pore volume v_p and the diameters in terms of the grain size δ. The injection rate was 0.3 pores/sec = 0.004 l/h, and the capillary number Ca $\simeq 2 \times 10^{-6}$. The exponent D, where $M/v_p \propto (2R/\delta)^D$, was determined to be $D = 2.7 \pm 0.1$.

be possible in this way to quantify unknown perturbations (at the borders of the range where the controlled perturbation governs the process) and extrapolate to the disturbance-free limit. This approach has been used with both gravity [50] and permeability gradients [51] as perturbations.

At higher rates growth takes place simultaneously all over the front at a more or less steady rate instead of the localized and sudden bursts observed during slow flow. The patterns become more centered around the injection point and denser. The two-dimensional patterns seem to form many loops at high as well as low injection rates. This is different from the patterns generated at high rates using high viscosity contrast fluids [17,18], where most of the growth occurs at tips and the branches almost never touch.

The crossover structures generated in the three-dimensional system at intermediate rates are highly ramified. In an earlier study [47] a characteristic length R_A was obtained as a measure of cluster linear size from the projected area A by setting $\pi R_A^2 = A$. R_A scaled with cluster mass M as $M \sim R_A^{D_A}$, with the exponent $D_A \simeq 2.5$. This value was found to be consistent with the exponent for three-dimensional diffusion-limited-aggregation clusters analyzed the same way. The second line in Fig. 3 is taken from one of the experiments analyzed previously [47].

The lower line in Fig. 3 show patterns generated during fast displacement in the three-dimensional system. The structures look very different from the ramified clusters obtained at lower injection rates. In contrast, these structures are ball-like, almost spherical, and have a rather sharp interface to the defending fluid phase. From this sharp interface thin "threads" of invading fluid extend out into the defending fluid. Whereas the advance of the main front is steady, these threads come in sudden localized bursts. The projections shown in Fig. 3 may give a misleading impression of the surface structure. The patterns in the second line (intermediate rate) were more ramified than they may appear in the projection shown. The sharp interface of the structures in the bottom line (high rate) was more evident when it was observed in the laboratory than the projections are able to show. These structures were fully developed for Ca $\geq 5 \times 10^{-3}$, but already the patterns with Ca $\geq 1 \times 10^{-3}$ were similar both qualitatively (they were quite spherical, but had rougher surfaces) and in quantitative estimates (discussed below); see Fig. 3 and the caption of Fig. 4.

Rather dense morphologies are to be expected during fast fluid-fluid displacement at low viscosity contrast. The most striking and surprising observation in these three-dimensional experiments is that the structure is so close to spherical and the interface is so sharp. This feature is less pronounced in the fast two-dimensional flows (bottom line of Fig. 2), but even here the patterns approach a circular shape with random offshoots. Some of the difference between two- and three-dimensional systems could be due to the different boundary conditions. In the two-dimensional system all of the rim is open to atmosphere, whereas only a thin channel around the top plate is open in three dimensions. In the previous study [47] patterns at intermediate rates resembled DLA patterns. Also the two-dimensional patterns at intermediate rates show features in common with DLA clusters (see the second line in Fig. 2). In comparison, the near compact structures generated at high displacement rates are surprising. It may be that the value for the viscosity ratio $m \simeq 14$ in our system leads to a particularly rich series of patterns as the injection rate is increased.

Stability arguments seem to predict instability for the present system. Peters and Flock [52] incorporate finite viscosity ratio, system size (an instability with wavelength larger than the system is irrelevant), and medium properties such as permeabilities and wettability, but not the pore level structure of the medium or interfacial tension, in a stability analysis for a cylindrical geometry. This argument predicts instability, quite clearly, for all the experiments in Fig. 4 (obviously caution should be exercised since the experiments in the present case had radial geometry). We take this as an indication that capillary effects may be important in determining the pattern morphology even at high displacement rates.

Visually, the three-dimensional ball structures gave an impression of being filled with invading fluid. However, comparison of the amounts of injected liquid to the apparent displacement structure volume (calculated from the diameter) indicated that the structures contain a large fraction of displaced fluid. The same conclusion was also reached by breaking one displacement structure into pieces. This was possible after the model had been kept for many hours at $-25\,^{\circ}$C. At this temperature the dibutyl-phthalate is a liquid whereas the sucrose solution froze and the structure could be dismantled. However, it was not possible to obtain details of the internal geometry or the saturation in this way. From data on injected fluid volumes and cluster sizes in seven fast dispacement experiments [spanned by Figs. 4(a)–4(d)] the saturation S

of invading fluid was determined to be $S = 0.42 \pm 0.02$. In other words, a surprisingly low fraction of the pore space inside these seemingly compact structures was filled with invading fluid. The values for S were determined in each experiment at the stage where the invasion structures filled half of the container. For the experiments in the first and second line of Fig. 3 saturations of 0.1 and 0.2 were estimated, respectively.

The values for the saturation S of the ball structures were determined in an alternative way from the fits in Fig. 4. Writing $M/\delta^3 = \tilde{A}(R/\delta)^D$, where M and R are the mass and the radius of the cluster and δ the grains size, the saturation is

$$S(R) = \frac{M/\delta^3}{\Phi\frac{4}{3}\pi(R/\delta)^3} = \frac{3}{4\pi\Phi}\tilde{A}\,(R/\delta)^{D-3} \qquad (3)$$

as function of radius. The fits in Fig. 4 were made according to $M/v_p = A(2R/\delta)^D$, where v_p is a characteristic pore volume (see Sec. II), so $\tilde{A}$ is related to the measured amplitudes A in a simple way. With $R/\delta = 37.5$ (the cluster fills about half of the container), and the measured values for A and D in the same seven experiments, a value $S = 0.47 \pm 0.04$ was obtained, consistent with the value above.

Measurements of the fractal dimension D for these structures gave $D = 2.6 - 3.0$; see Fig. 4. The dimensions determined this way should be taken as estimates since the range in sizes is small. There was also some uncertainty in the determination from photographs of precisely when the injection started in these fast experiments. However, these values for D are consistent with rather dense patterns that still contain much of the displaced fluid. Further, the values are higher than $D \simeq 2.5$, found for the ramified structures at intermediate rates. Using the same seven fast experiments as above, an average value of $D = 2.74 \pm 0.16$ was determined. Also the S values given above indicate that denser structures are generated as rate is increased.

The nature of the structures seems to be stable to perturbations of the flow field. Figure 6 (middle line) shows elongated structures generated in an experiment in which a top plate with many holes in it was used. As indicated in Fig. 6, the pattern tends to grow more in the (easy) upward direction than in the standard experiments. But the structure surface still shows the same features; it is sharp with threadlike offshoots. After a fast experiment was completed the generated structures could be kept essentially unchanged in the laboratory for many days.

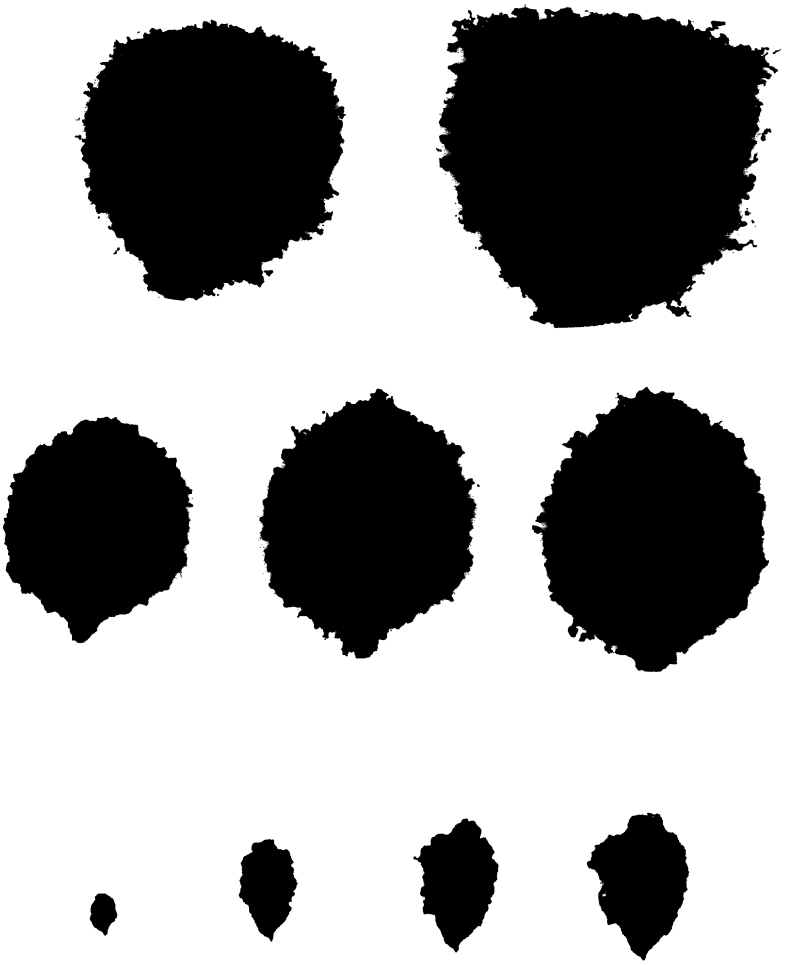

FIG. 6. Displacement structures in this figure illustrate various limitations of the experimental technique used. Each line shows several stages in the same experiment. The experiment in the upper line was carried out with the standard setup described in Sec. II. The patterns shown are from late stages of the fastest experiment [bottom line in Figs. 3 and 4(d)]. The rightmost structure fills about 80% of the glass container, almost touches the top plate, and deviates from a spherical shape. In the experiment in the middle line a perforated top plate (see Fig. 1) was used. This leads to a more asymmetric flow field and more distorted shapes. The rightmost structure in this experiment is very close to the top plate. The lower line illustrates what happens if there is no loaded top plate at all during a fast experiment. Part of the medium is lifted and a jet develops upward from the injection point. The scale for these three series of structures is close to identical, so the pattern sizes may be directly compared.

The discussion above may indicate that the structures are close to compact. But there is also the possibility that they have dense radial morphologies and perhaps also fractal geometry. Dense radial patterns are generated in some modified DLA models [53, 54] (as well as several different physical systems). In a radially biased DLA model [54] the dense patterns had the same fractal dimension D as the unbiased ones and all the striking changes in morphology were accounted for by the amplitude A ($M = AR^D$). In analogy it is conceivable that fluid-fluid displacement structures have a fractal dimension $D = 2.5$, which is the value for three-dimensional DLA clusters. Grier *et al.* [55] have argued that a resistivity, no matter how small, along the growth "channels" of the structure should give rise to dense, radial patterns, and a similar idea may apply to viscous resistance along (possible) long, thin fingers in the present case. An important feature of the present system, however, is the existence of threshold values for growth (invasion) along the finger due to the pinned interface. The invading fluid might overcome these thresholds at high injection rates (with large viscous pressure drops), giving rise to a compactification of the structure. This may explain the ramified DLA-like patterns observed at intermediate displacement rates [47] since the pressure drop in the invading fluid structure in this case is too small that most of the threshold values can be overcome. On the other hand, the Reynolds numbers (see caption to Fig. 4, $\mathrm{Re} = \rho v \delta / \mu_i$, where ρ and μ_i are density and viscosity, respectively, of the invading fluid and δ the grain size) indicate that inertia forces dominate over viscous forces, at least in the fastest experiments. A different prediction comes from a real space renormalization group calculation [56]. It was found that for any finite viscosity contrast the pattern will eventually cross over to compact growth. However, a medium without structure was assumed in that study; thus all pore level mechanisms were neglected.

V. SUMMARY

Fluid-fluid displacement patterns generated in large, three-dimensional porous media at a series of different flow rates at a low viscosity contrast have been visualized. The limiting morphology in fast displacement ($\mathrm{Ca} \geq 5 \times 10^{-3}$) was found to be ball-like and rather dense structures. Still these structures contain much of the displaced fluid. Reference experiment in two dimensions showed a similar behavior. The experiments may indicate that capillary effects are important in determining the pattern morphology also at high displacement rates since the pressure drops in the two phases are comparable. The nature of the patterns formed during fast, immiscible fluid-fluid displacement in porous media at a finite viscosity ratio is still not fully understood and there is a need for more theoretical and experimental studies.

ACKNOWLEDGMENTS

This research has been supported by VISTA, a research cooperation between the Norwegian Academy of Science and Letters and Den norske stats oljeselskap a.s. (STATOIL), and by NFR, the Norwegian Research Council for Science and the Humanities.

[1] J. Bear, *Dynamics of Fluids in Porous Media* (Dover, New York, 1972).
[2] J. Bear and Y. Bachmat, *Introduction to Modeling of Transport Phenomena in Porous Media* (Kluwer, Dordrecht, 1990).
[3] F. A. L. Dullien, *Porous Media: Fluid Transport and Pore Structure* (Academic, New York, 1979).
[4] J. Feder, *Fractals* (Plenum, New York, 1988).
[5] M. Sahimi, Rev. Mod. Phys. **65**, 1393 (1993).
[6] P. G. de Gennes and E. Guyon, J. Mec. **17**, 403 (1978).
[7] R. Lenormand and S. Bories, C. R. Acad. Sci. Paris Ser. B **291**, 279 (1980).
[8] R. Chandler, J. Koplik, K. Lerman, and J. F. Willemsen, J. Fluid Mech. **119**, 249 (1992).
[9] P. G. de Gennes, Phys. Chem. Hydrodyn. **4**, 175 (1983).
[10] D. Wilkinson and J. F. Willemsen, J. Phys. A **16**, 3365 (1983).
[11] R. Lenormand and C. Zarcone, Phys. Rev. Lett. **54**, 2226 (1985).
[12] L. Furuberg, J. Feder, A. Aharony, and T. Jøssang, Phys. Rev. Lett. **61**, 2117 (1988).
[13] S. Roux and E. Guyon, J. Phys. A **22**, 3693 (1989).
[14] K. J. Måløy, L. Furuberg, J. Feder, and T. Jøssang, Phys. Rev. Lett. **68**, 2161 (1992).
[15] T. A. Witten and L. M. Sander, Phys. Rev. Lett. **47**, 1400 (1981); Phys. Rev. B **27**, 5686 (1983).
[16] L. Paterson, Phys. Rev. Lett. **52**, 1621 (1984).
[17] J.-D. Chen and D. Wilkinson, Phys. Rev. Lett. **55**, 1892 (1985).
[18] K. J. Måløy, J. Feder, and T. Jøssang, Phys. Rev. Lett. **55**, 2688 (1985).
[19] E. L. Hinrichsen, K. J. Måløy, J. Feder, and T. Jøssang, J. Phys. A **22**, L271 (1989).
[20] D. Y. C. Chan, B. D. Hughes, and L. Paterson, Phys. Rev. A **34**, 4079 (1986).
[21] K. J. Måløy, J. Feder, T. Jøssang, and P. Meakin, Phys. Rev. A **36**, 318 (1987).
[22] L. A. Turkevich and H. Scher, Phys. Rev. Lett. **55**, 1026 (1985).
[23] P. Meakin, H. E. Stanley, A. Coniglio, and T. A. Witten, Phys. Rev. A **32**, 2364 (1985).
[24] J. F. Fernández, R. Rangel, and J. Rivero, Phys. Rev. Lett. **67**, 2958 (1991).
[25] J. D. Sherwood and J. Nittmann, J. Phys. (Paris) **47**, 15 (1986).
[26] J. D. Sherwood, J. Phys. A **19**, L195 (1986).
[27] J. D. Sherwood, J. Comput. Phys. **68**, 485 (1987).
[28] A. J. DeGregoria, Phys. Fluids **28**, 2933 (1985).
[29] A. J. DeGregoria, Phys. Fluids **29**, 3557 (1986).
[30] P. R. King, J. Phys. A **20**, L529 (1987).

[31] M. Blunt and P. King, Phys. Rev. A **42**, 4780 (1990).
[32] M. Blunt and P. King, Transp. Porous Media **6**, 407 (1991).
[33] H. H. Hardy, Society of Petroleum Engineers Report No. 15495, 1986 (unpublished).
[34] M. Sahimi and Y. C. Yortsos, Phys. Rev. A **32**, 3762 (1985).
[35] L. Paterson, J. Phys. A **20**, 2179 (1987).
[36] M. J. King and H. Scher, Phys. Rev. A **35**, 929 (1987).
[37] D. F. Leclerc and G. H. Neale, J. Phys. A **21**, 2979 (1988).
[38] T. Nagatani, J. Phys. A **21**, 1109 (1988).
[39] H. Sideiqui and M. Sahimi, J. Phys. A **23**, L497 (1990); Chem. Eng. Sci. **45**, 163 (1990).
[40] T. Nagatani and H. E. Stanley, Phys. Rev. A **43**, 2963 (1991)
[41] L. W. Ni, V. Hornof, and G. Neale, Rev. Inst. Fr. Pet. **41**, 217 (1986).
[42] R. Lenormand and C. Zarcone, Phys. Chem. Hydrodyn. **6**, 497 (1985).
[43] R. Lenormand, C. R. Acad. Sci. Paris Ser. II **301**, 247 (1985).
[44] R. Lenormand, E. Touboul, and C. Zarcone, J. Fluid Mech. **189**, 165 (1988).
[45] V. Frette, K. J. Måløy, F. Boger, J. Feder, T. Jøssang, and P. Meakin, Phys. Scr. **T38**, 95 (1991).
[46] R. L. Chuoke, P. van Meurs, and C. van der Poel, Pet. Trans. AIME **216**, 188 (1959).
[47] V. Frette, K. J. Måløy, F. Boger, J. Feder, T. Jøssang, and P. Meakin, Phys. Rev. A **42**, 3432 (1990).
[48] In previous work [45, 47] a value $\sigma = 23\,\mathrm{dyn/cm}$ was obtained using a different measurement technique. The correct estimate from those measurements is $18 \pm 3\,\mathrm{dyn/cm}$, which is consistent with the drop weight value. The estimate $\sigma = 13 \pm 1.5\,\mathrm{dyn/cm}$ was based on many more measurements and is considered to be more reliable.
[49] A. W. Adamson, *Physical Chemistry of Surfaces* (Wiley, New York, 1976).
[50] V. Frette, J. Feder, T. Jøssang, and P. Meakin, Phys. Rev. Lett. **68**, 3164 (1992); P. Meakin, J. Feder, V. Frette, and T. Jøssang, Phys. Rev. A **46**, 3357 (1992).
[51] M. Chaouche, N. Rakotomalala, D. Salin, B. Xu, and Y. C. Yortsos, Phys. Rev. E **49**, 4133 (1994).
[52] E. J. Peters and D. L. Flock, Soc. Pet. Eng. J. **21**, 249 (1981).
[53] R. Voss, Fractals **1**, 141 (1993).
[54] P. Meakin, J. Feder, and T. Jøssang, Phys. Rev. A **43**, 1952 (1991).
[55] D. G. Grier, D. A. Kessler, and L. M. Sander, Phys. Rev. Lett. **59**, 2315 (1987).
[56] J. Lee, A. Coniglio, and H. E. Stanley, Phys. Rev. A **41**, 4589 (1990).

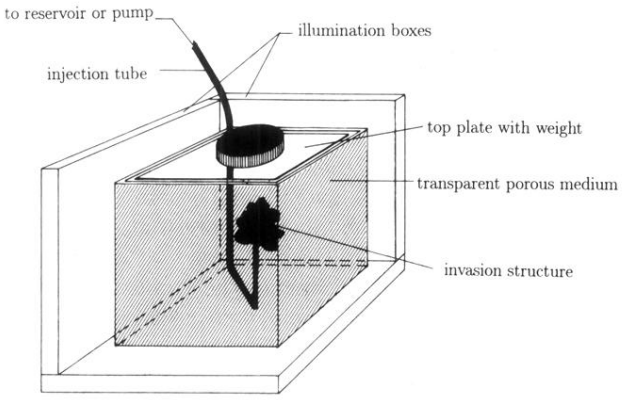

FIG. 1. Experimental setup. A transparent porous medium is held in a glass container. The plate on top of the medium is loaded with a weight to prevent grain movements during the displacement processes. The system is illuminated from below and through two adjacent faces. Two projections of the patterns that are generated when a second fluid is injected are photographed.

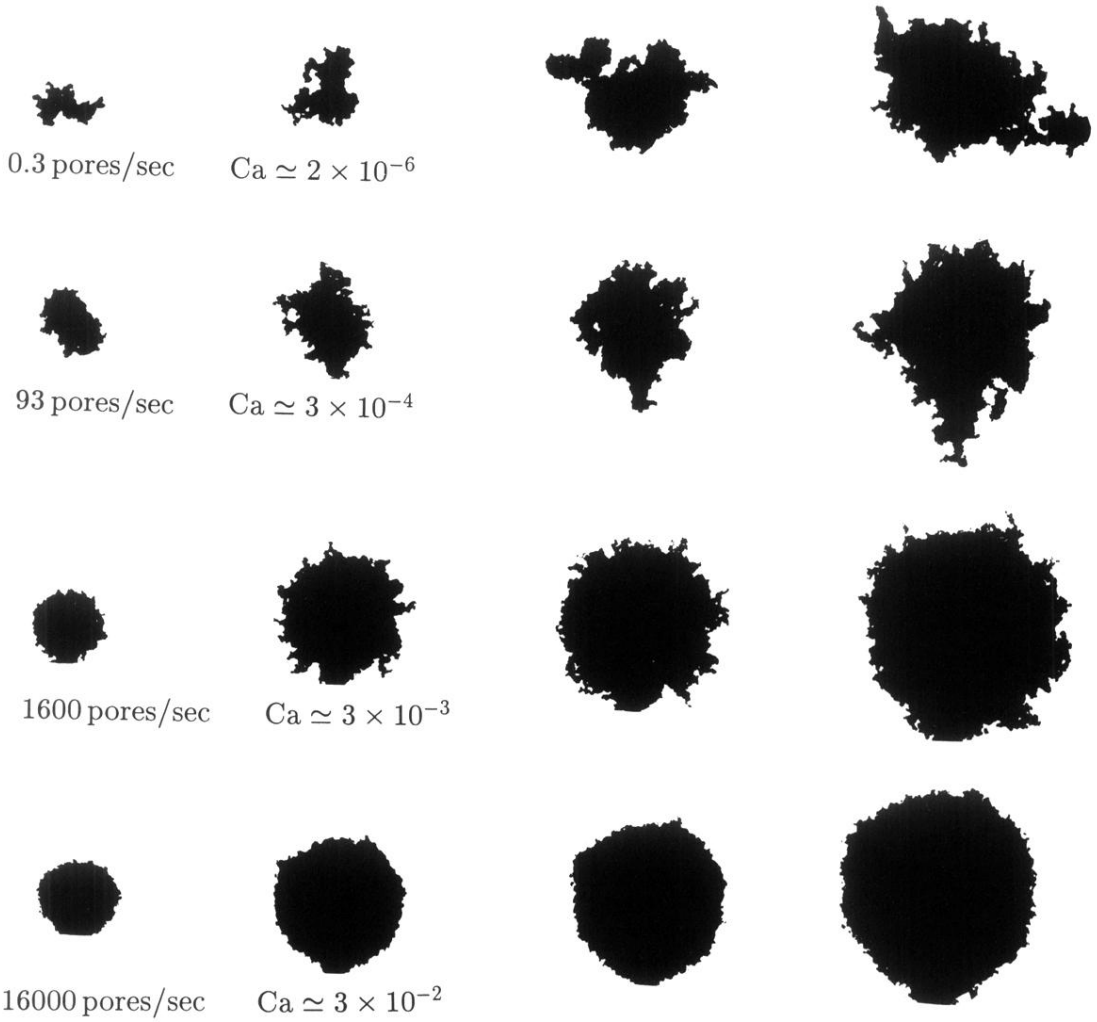

FIG. 3. Fluid-fluid displacement patterns generated in a three-dimensional porous medium. Each line show several stages in one experiment. The injection rates and the values of the capillary number Ca are given in each case. The physical flow rates were 0.004, 1.24, 21, and 210 l/h.

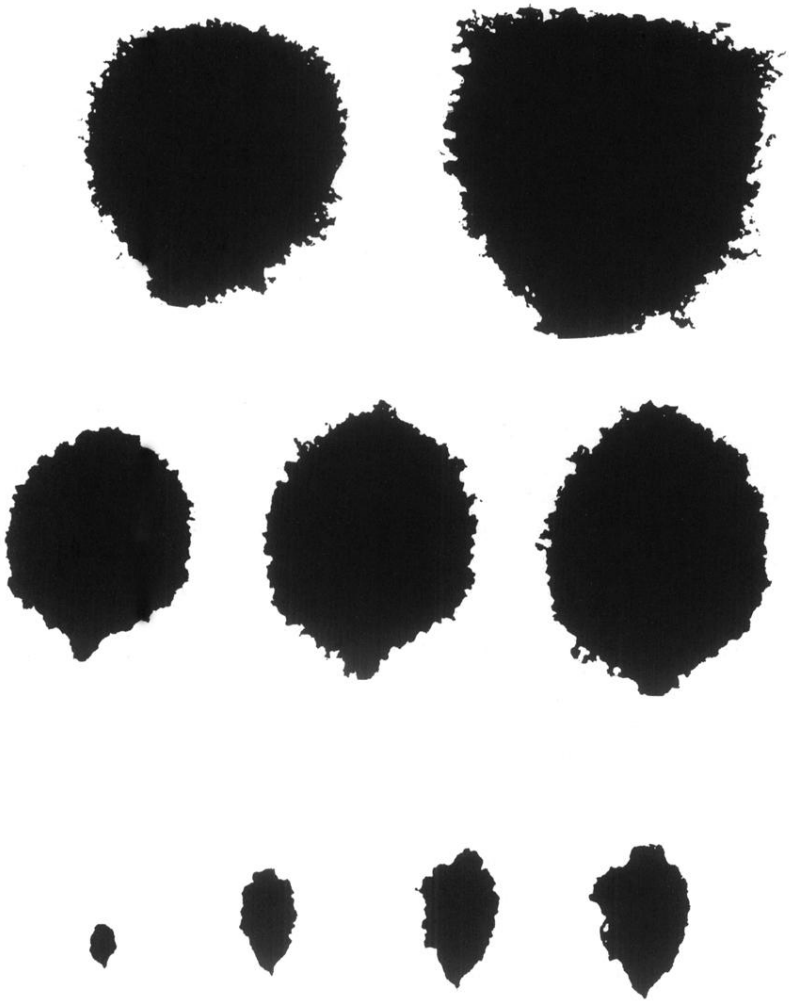

FIG. 6. Displacement structures in this figure illustrate various limitations of the experimental technique used. Each line shows several stages in the same experiment. The experiment in the upper line was carried out with the standard setup described in Sec. II. The patterns shown are from late stages of the fastest experiment [bottom line in Figs. 3 and 4(d)]. The rightmost structure fills about 80% of the glass container, almost touches the top plate, and deviates from a spherical shape. In the experiment in the middle line a perforated top plate (see Fig. 1) was used. This leads to a more asymmetric flow field and more distorted shapes. The rightmost structure in this experiment is very close to the top plate. The lower line illustrates what happens if there is no loaded top plate at all during a fast experiment. Part of the medium is lifted and a jet develops upward from the injection point. The scale for these three series of structures is close to identical, so the pattern sizes may be directly compared.